Proceedings of the
Annual Stability Conference
Structural Stability Research Council
San Antonio, Texas, March 21-24, 2017

Stability and moment-rotation behavior of cold-formed steel purlins with sleeved bolted connection

Fernando H. S. Gilio[1], Luiz C. M. Vieira Jr.[2], Maximiliano Malite[3]

Abstract

Long runs of cold-formed steel Z-section purlins are often segmented due to assemblage and transportation issues. The segments are commonly connected by bolts to a short cold-formed steel member similar to the purlin; this short member is typically called a sleeve; from a structural point of view, it does not guarantee a state of full continuity to the purlin. This study reports a series of 15 experiments on cold-formed steel Z-sections purlins with sleeved bolted connections tested in bending. These experiments vary cross-section height, thickness and length of sleeve, and span. This parametric experimental study seeks to better understand the flexural-buckling strength, collapse mechanism, and moment-rotation behavior of purlin-sleeve systems. Since the design of purlins with sleeved bolted connections is often limited by the serviceability limit state, in this case excessive displacement, special attention is given to accurately determining and understanding the moment-rotation behavior of purlin-sleeve systems. Based on the experimental results, an expression is proposed to predict non-linear moment-rotation behavior; the proposed expression is compared to expressions previously proposed in the literature. The proposed moment-rotation expression, when used in a simple rotation spring-beam model, leads to accurate prediction of displacement in the purlin-sleeve system.

1. Introduction

Multi-span purlins are usually connected by overlapping by a short segment or through a separate element, a sleeve. Both types of connection are attained by bolting together the web of juxtaposed purlins or juxtaposed purlin-sleeve. The sleeve connection is usually assembled on the supporting frame; erectors consider sleeve connections easier and faster to assemble compared to overlapped connections.

[1] PhD Student, University of Sao Paulo – EESC, Sao Carlos, Brazil, <fhg.engenharia@gmail.com>
[2] Assistant Professor, University of Campinas, Campinas, Brazil, <vieira@fec.unicamp.br>
[3] Associate Professor, University of Sao Paulo – EESC, Sao Carlos, Brazil, <mamalite@sc.usp.br>

Moore (1990) characterizes the non-linear moment-rotation behavior of cold-formed steel purlins with sleeved bolted connections. Bryan (1993) proposes a mechanical model to define the rotational stiffness (K_ϕ) of sleeved bolted connections with four bolts, which results in Eq. 1a; this expression is related to the bearing stiffness at the bolt hole (K_h), which is determined from a lap shear test, Eq. 1b.

$$K_\phi = \frac{M}{\phi} = 4K_h r^2 \quad \left(kN.mm/rad\right) \tag{1a}$$

$$K_h = \frac{1000}{5n\left(\frac{10}{t_1}+\frac{10}{t_2}-2\right)} \quad \left(kN/mm\right) \tag{1b}$$

where r is the distance between the center, defined by the four bolts, and each bolt hole, t_1 and t_2 are the thicknesses of the connected profiles (t_1 < 8 mm and t_2 < 8 mm) and n is a factor that depends on the shear plane position, number of bolts, and connection type.

Gutierrez et al. (2011) conclude from their experimental study that bending strength and rotational stiffness of purlins with sleeved bolted connections are lower than for continuous purlins. Following a previous study, Yang and Liu (2012), Gutierrez et al. (2015) and Fávero et al. (2016) propose a simplified Beam-Spring Model (BSM) for displacement prediction of multi-span purlin systems. The present paper aims to better understand the flexural-buckling strength, collapse mechanism, and moment-rotation behavior of purlin-sleeve systems through a parametric experimental study.

2. Sleeved Connection Experiments

The methodology used in this experimental study was first proposed by Ghosn and Sinno (1996). Based on the moment diagram of a continuous purlin (Fig. 1a) with uniformly distributed load, an idealized simply supported beam with a concentrated load at mid-span is defined (Fig. 1c) to approximately represent the moment diagram between inflection points at the support area. The inflection points are located at 21% to 25% of the span (L) from the maximum moment (M_{max}); to test the region between inflection points, a total length of 50% of the span (L) is defined as the length necessary to carry out the experiment (L_t). The internal support is replaced by a concentrated force (F) introduced at mid-span, which represents the vertical support reaction. In each experiment, two beams (sleeve and purlin system) are assembled and braced to each other by the web; thus, each beam is prevented from buckling laterally.

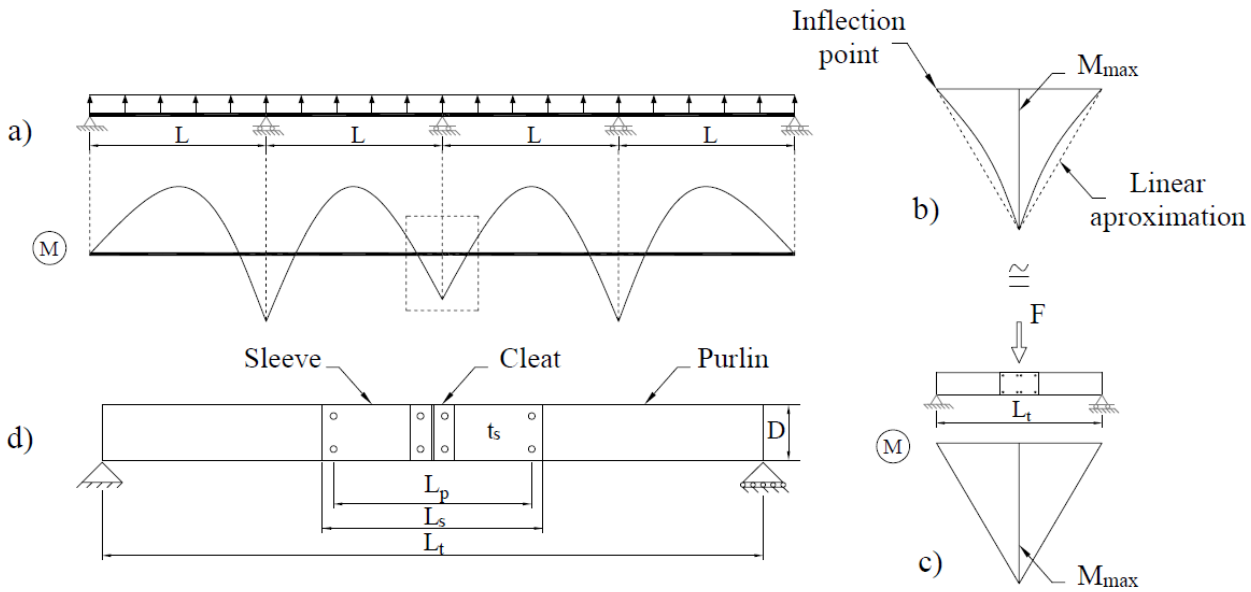

Figure 1: Idealization of test setup: a) continuous beam with uniformly distributed load and moment diagram of a continuous purlin; b) linear approximation of moment diagram; c) equivalent simply supported beam; and d) variables to be parametrically investigated. (Adapted from: Fávero et al., 2016).

3. Parametric Experimental Program

A series of 15 laboratory tests, as depicted in Fig. 1, were conducted on cold-formed Z-sections. The main goal was to investigate the influence on the structural behavior of sleeved connections given different: (i) sleeve effective length (L_p); (ii) cross-section height (D); (iii) experiment span (L_t); and (iv) sleeve thickness (t_S), as in Fig. 1d.

Table 1 summarizes the experimental program; the experiments were subdivided into three series, identified as A, B, and C. In each series, the ratio Lp/D assumes values of 2, 4, 6, and a continuous purlin (ratio Lp/D is non-existent and the experiment is carried out as a simply supported beam experiment); in addition, the ratio Lp/Lt may vary from 7.33% (short sleeve) to 31.5% (long sleeve). Series B and C also counted with additional experiments where the sleeve thickness (3 mm) differs from the cross-section thickness (1.95 mm), and an experiment connected only by the cleat (ZB63-S) was added to series B.

In addition to the experimental program presented herein, the authors compared their data to experiments carried out by Fávero Neto et al. (2016): this forms experiment series D and E, in which cross-section thickness assumes values of 1.75 mm (Z1-L5) and 2.70 mm (Z2-L5), respectively. The corresponding continuous purlin experiments (Z1-C e Z2-C) are included in Table 1.

Table 1: Description and dimensions of the experimental program

Series	Experiment	Cross-section height (D) (mm)	Cross-section thickness (t) (mm)	Sleeve effective lenght (L_p) (mm)	Experiment span (L_t) (mm)	Moment of inertia (I)[c] (mm^4)	Ratio L_p/D	Ratio L_p/L_t (%)
A	ZA62-L44	220	1.95	440	6000	4,969,244	2	7.33
	ZA62-L88			880		4,995,331	4	14.67
	ZA62-L132			1320		5,003,251	6	22.00
	ZA62-C			-		4,991,595	-	-
B	ZB63-L63	315	1.95	630	6000	13,273,885	2	10.50
	ZB63-L126			1260		13,408,901	4	21.00
	ZB63-L126T3[b]			1260		13,508,115	4	21.00
	ZB63-L189			1890		13,456,586	6	31.50
	ZB63-S			-		13,532,107	-	-
	ZB63-C			-		13,403,682	-	-
C	ZC83-L63	315	1.95	630	8000	13,463,273	2	7.88
	ZC83-L126			1260		13,569,931	4	15.80
	ZC83-L126T3[b]			1260		13,484,462	4	15.80
	ZC83-L189			1890		13,532,107	6	23.62
	ZC83-C			-		13,430,749	-	-
D[a]	ZD62-L1036 (Z1-L5)	270	1.75	1036	6000	8,032,393	3.84	17.27
	ZD62-C (Z1-C)			-		8,031,887	-	-
E[a]	ZE62-L1036 (Z2-L5)	270	2.70	1036	6000	12,770,985	3.84	17.27
	ZE62-C (Z2-C)			-		12,398,641	-	-

[a]D and E series refer to Fávero Neto (2013).

[b]Sleeve thickness and moment inertia are 3.00 mm and 20,747,828 mm^4, respectively.

[c]Calculated based on the real dimensions measured at the laboratory, excluding the zinc coating.

Legend for identifying prototypes

Z B 8 3 - L 126 T3
① ② ③ ④ ⑤ ⑤.1 ⑤.2

1 - Z section
2 - Series denomination (A, B or C)
3 - Experiment span (6 mm = 6000 8 = 8000 mm)
4 - Cross-section height (2 = 220 or 270 mm and 3 = 315 mm)
5 - Connection type (C = continuous, L = sleeve, and S = without sleeve)
5.1 - Sleeve effective lenght (L_p)
5.2 - Sleeve thickness (T3 = 3 mm)

4. Steel Properties

Three steel coupon tests were carried out, one for each experiment series. The material used to manufacture the purlins is denominated ZAR345 steel by ABNT (2010), with standard zinc-coating thickness of 0.02 mm on each side of the steel plate. The coupon tests were carried out according to ASTM A370 (2014); the yield stress (f_y) and ultimate stress (f_u) values are summarized in Table 2.

Table 2: Coupon test results (height/thickness refers to the nominal cross-section measurements of each series of experiments)

Height/thickeness (mm)[a]	f_y (MPa)	f_u (MPa)
220/1.95	396.0	484.9
315/1.95	381.1	473.7
315/3.00	373.1	462.3

[a]Nominal values.

Bolts, nuts and washers used in the experiments are defined as M16 by ASTM A325 (2013) specification. The hole-size diameter is equal to the bolt diameter added by 4 mm.

5. Experimental Results – Loading-Displacement Curves

Fig. 3 depicts the loading-displacement curves for the series A, B, and C experiments. For comparison purposes, Fig. 3, also plots the displacement solution for a linear-elastic analysis of a simply supported continuous beam with a concentrated force at mid-span (displacement = $FL_t^3/(48EI)$); Young's modulus is considered equal to 200,000 MPa, F is the concentrated force at mid-span, and I is moment of inertia for the nominal cross-section dimensions. As the ratio Lp/D is increased, the sleeve-purlin systems show results closer to the simply supported continuous beam experiment and equation for a linear-elastic analysis, as in Fig. 3. For small increments of force, there is a significant change in the displacements measured in experiment ZB63-S (Fig. 3b), which shows that although the cleat has reduced capacity to promote continuity, it is responsible for a small amount of the bending stiffness of the purlin-sleeve connection.

Gutierrez et al. 2011, Yang and Liu (2012), and Ye et al. (2013) attribute excessive deformation of the holes region to a significant parcel of connection flexibility. All connections in the present experiments, however, were disassembled after testing and the hole dimensions measured; hole deformation is considered negligible for the purlin-sleeve system experiments. Fig. 2 depicts a connection sample after testing; it is visually apparent that there is no major deformation at the holes region.

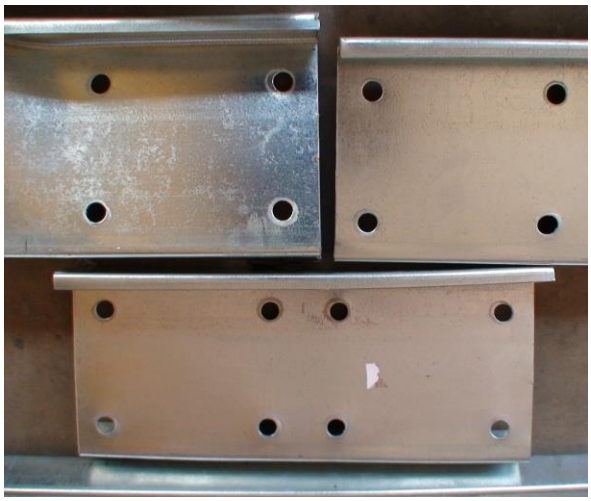

Figure 2: Hole deformation after testing experiment ZA62-L44

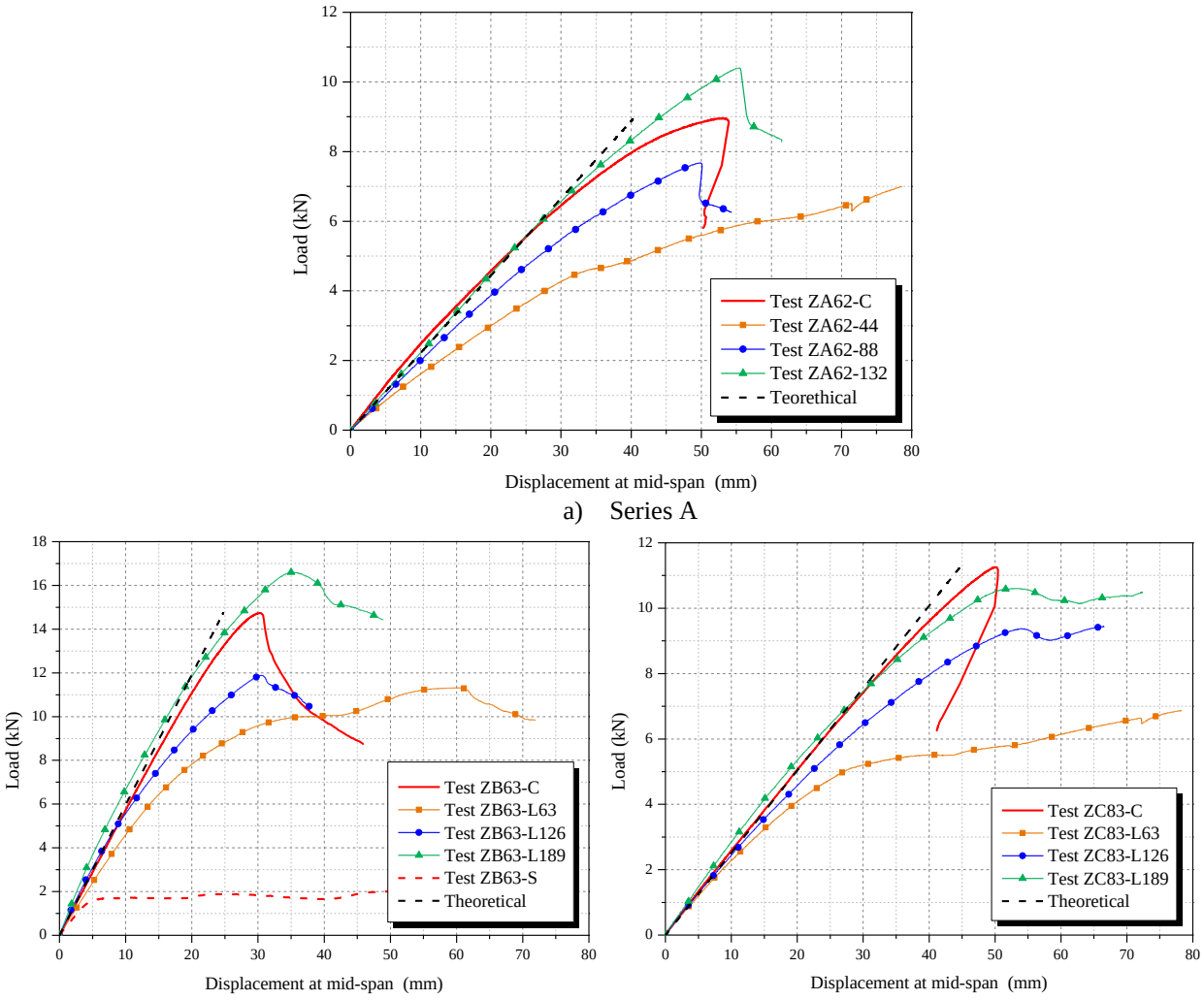

a) Series A

b) Series B

c) Series C

Figure 3: Mid-span load-displacement curves

6. Rotation Spring-Beam Model

A finite element (FE) model was generated using ANSYS (2013) to numerically analyze the sleeve-purlin system. The FE model consists of combining classic beam elements (BEAM3) with non-linear rotational springs (COMBIN39). At the sleeve region, the beam moment of inertia was doubled, assuming that there is full interaction between purlin and sleeve; also, shear deformation of the beam elements was ignored. This FE model is referred to in this paper as the BSM.

Five position transducers were placed in each experiment; all displacements and rotations experimentally measured have the subscript "Total", and a superscript indicating the section where the measurement was taken, as in Fig. 4a. The numerical simulation of each experiment was subdivided into two numerical simulations: (i) the rotation spring simulating the purlin-sleeve connection has infinite stiffness and all vertical displacement is due to bending deformation of the purlin member (I_p) and sleeve-purlin member (I_s), as in Fig. 4b; and (ii) the

bending stiffness of all members is infinite, while the rotational spring stiffness is equal to the actual purlin-sleeve connection stiffness, thus, only rigid-body movement is allowed, as in Fig. 4c. This simulation strategy thus assumes that the vertical displacement of the purlin-sleeve system can be approximated by adding the vertical displacement in cases (i) and (ii).

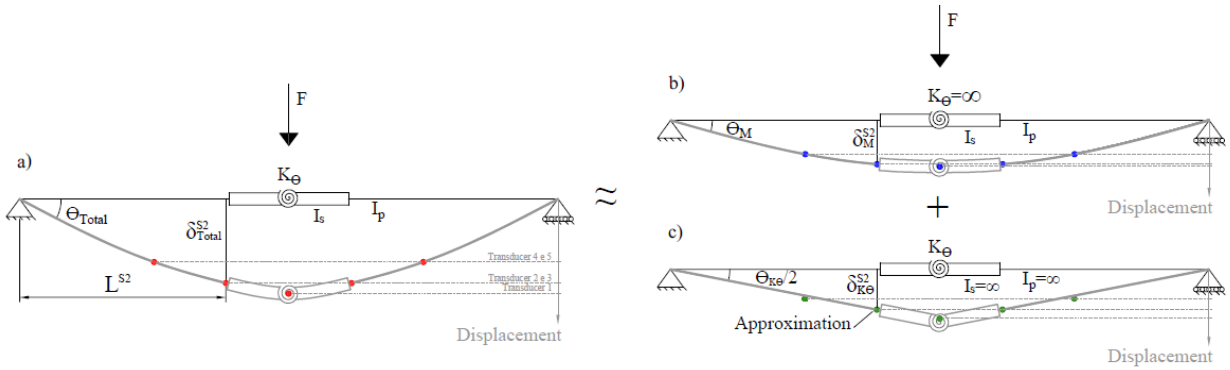

Figure 4: Superposition adopted in modeling the purlin-sleeve systems. Position transducer 1 is placed at mid-span, position transducers 2 and 3 are placed at the end of the sleeve, and position transducers 4 and 5 are placed 1500 mm from the mid-span.

This simple strategy of separating the vertical displacement into two parcels makes it possible to analyze the rotational spring separately, without taking into account the members' bending stiffness. One can easily realize from the free-body diagram depicted in Fig. 4, that, for example, the displacement at section 2, S2, due to the contribution of rotational spring can be expressed by Eq. 2a, the rigid-body rotation at the support is given by Eq. 2b, and the rotational spring stiffness is given by Eq. 2c, where M is the bending moment at mid-span.

$$\delta^{S2}_{K\theta} = \delta^{S2}_{Total} - \delta^{S2}_{M} \tag{2a}$$

$$\theta_{K\theta} = \frac{2\delta^{S2}_{K\theta}}{L^{S2}} \tag{2b}$$

$$K_\theta = \frac{M}{\theta_{K\theta}} \tag{2c}$$

Fig. 5a depicts the moment-rotation curve determined for experiment ZB63-L126; this curve is used as input information to define the non-linear rotational springs (COMBIN39) in ANSYS (2013). In Fig. 5b, the experimental load-displacement curves for all five position transducers of experiment ZB63-L126 are compared with the results obtained with the FE model (BSM); the FE model leads to satisfactory results when compared to the experiments.

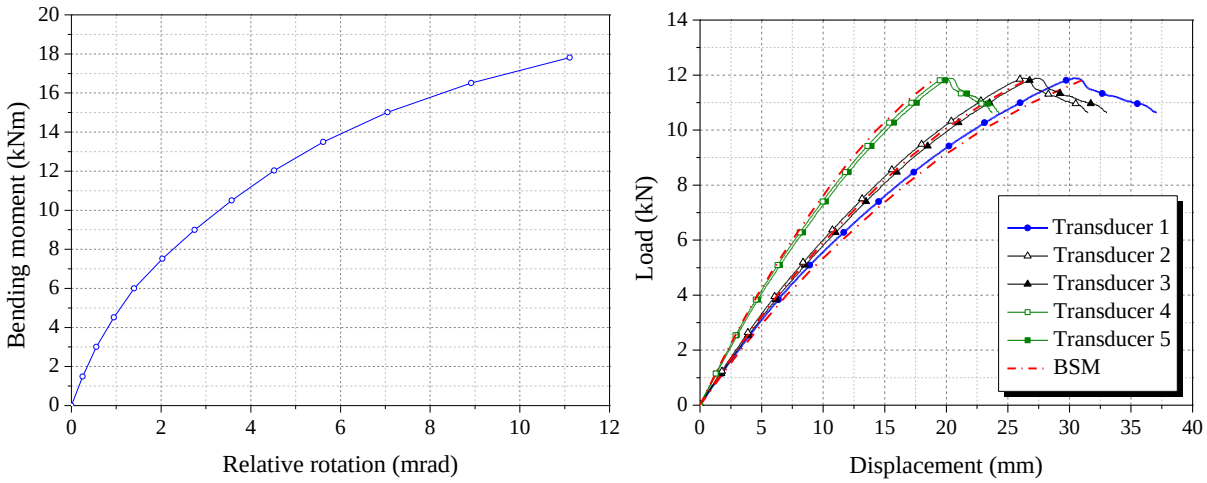

a) Moment-rotation behavior of rotational spring K_Θ b) Experimental and numerical load- displacement

Figure 5: Experiment ZB63-L126

7. Moment-Rotation Curves

In Fig. 6, bending moment and relative rotation, also known as moment-rotation, curves are depicted according to the ratio Lp/D (sleeve effective length / cross-section height). Comparing series A to B (different cross-section height), it is clear that by increasing the cross-section height, the moment-rotation stiffness also increases; however, comparing series B to C (different experiment span), it is evident that for Lp/D ratios of 4 and 6, the moment-rotation stiffness presents small changes. The large difference between series C and B in Fig. 6a is due to a change in the failure mechanism; specimen ZC83-L63 developed a plastic mechanism at the end of the sleeve (Fig. 13), which led to a loss of stiffness above a bending moment of 10 kNm.

As depicted in Fig. 6, moment-rotation curves are governed by a non-linear relationship. This relationship can be satisfactorily approximated by the exponential curve given in Eq. 3 as a function of bending moment (M) or relative rotation (θ).

$$M = \alpha r\left(1-e^{-\beta Dr\theta}\right)=\frac{FL_t}{4} \quad \text{or} \quad \theta = \frac{1}{\beta Dr}\ln\left(\frac{\alpha r}{\alpha r - M}\right) \tag{3}$$

where:

F is the mid-span force;

α = -15.42L_p/D + 123.03 when $2 \leq L_p/D \leq 4$;

α = [16.45(1-L_t/6)-1.43]L_p/D + [67.10-65.77(1-L_t/6)] when $4 < L_p/D \leq 6$;

β = -0.59L_p/D + 5.20 when $2 \leq L_p/D \leq 6$;

$r = 0.5(a^2 + c^2)^{0.5}$, defined in Fig. 7;

L_t,L_s,L_p and D are defined in the Fig. 1d;

L_p, D, L_t and r must be defined in meters, M in kN.m, F in kN, and θ in mrad.

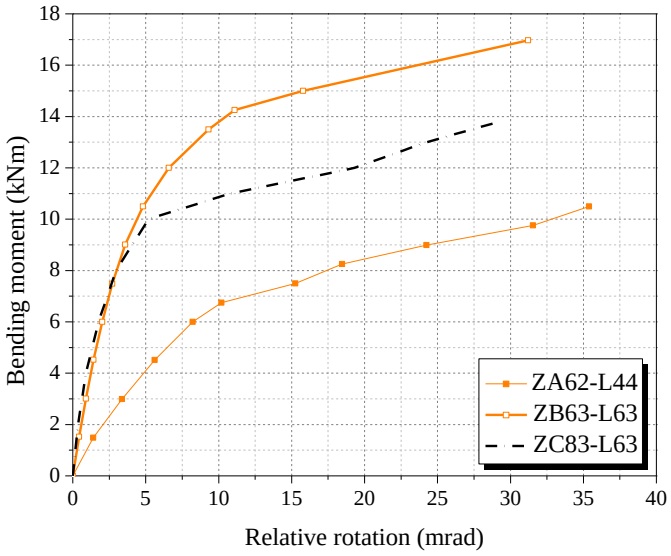

a) Ratio $L_p/D = 2$

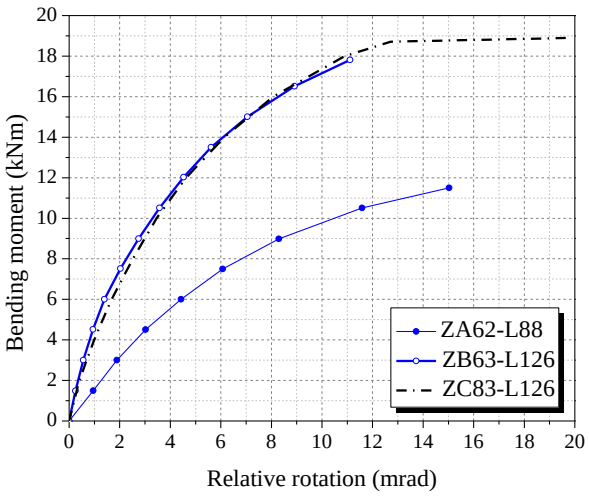

b) Ratio Lp/D = 4

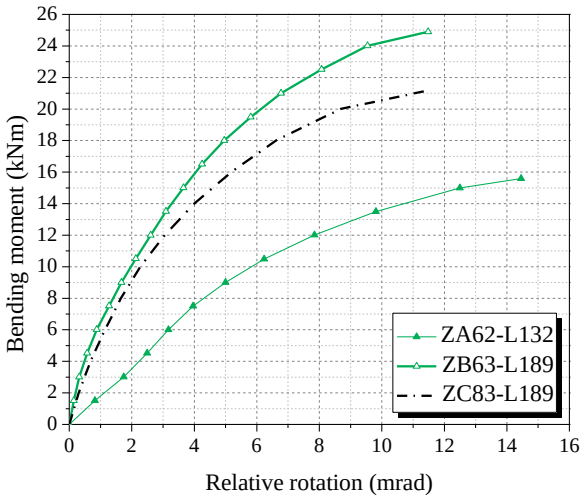

c) Ratio Lp/D = 6

Figure 6: Moment-rotation curves for sleeved bolted connection

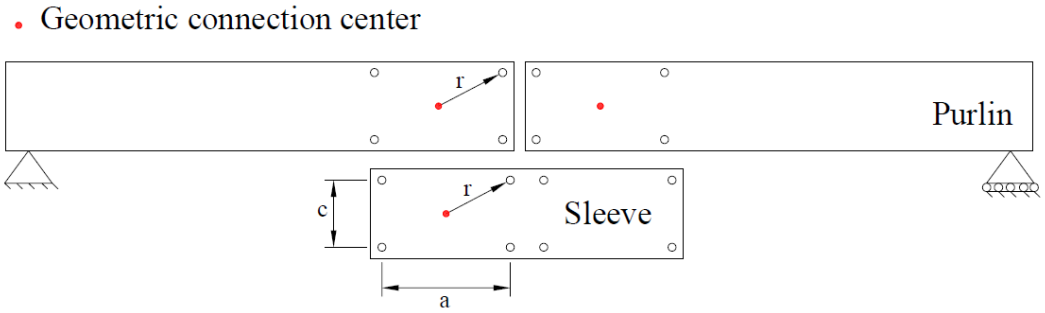

Figure 7: Variables *a*, *c* and *r* in the sleeve connection

Thus, non-linear rotational stiffness (K_θ) is given by Eq. 4.

$$K_\theta = \frac{M}{\theta} = \frac{FL_t \beta Dr}{4\ln\left(\frac{\alpha r}{\alpha r - M}\right)} \tag{4}$$

Based on the BSM depicted in Fig. 4a, displacement at mid-span can be calculated using Castigliano's theorem, where total displacement at mid-span (δ_{Total}) is given by the partial derivative of the internal strain energy U_i with respect to the concentrated force at mid-span F. The internal strain energy U_i is defined in Eq. 5.

$$U_i = 2\int_0^{(L_t - L_s)/2} \frac{M_L^2}{2EI_p} dx + 2\int_{(L_t - L_s)/2}^{L_t/2} \frac{M_L^2}{2EI_s} dx + \frac{K_\theta \theta^2}{2} \tag{5}$$

where:
E is Young's modulus (200,000 MPa);
I_s is sleeve-purlin moment of inertia;
I_p is purlin moment of inertia.

Since the system is equivalent to a simply supported beam, the bending moment (M_L) is given by Fx/2, where $0 \leq x \leq L_t/2$; thus, total displacement at mid-span (δ_{Total}) is given by Eq. 6.

$$\frac{\partial Ui}{\partial F} = \delta_{Total} = \frac{2F\left(L_t - L_s\right)^3}{96EI_p} + \frac{2FL_t^3}{96EI_s} - \frac{2F\left(L_t - L_s\right)^3}{96EI_s} + \frac{2FL_t^2}{32K_\theta} \tag{6}$$

In Eq. 6, the three first terms are due to a linear analysis (δ_{Linear}), while the last term is the non-linear component ($\delta_{Nonlinear}$) of the analysis; the last term can be further simplified by substituting K_θ given in Eq. 4. Thus, total displacement at mid-span (δ_{Total}) is given by the sum of displacements from a linear and a non-linear analysis, Eq. 7, which can be decoupled into Eq. 8 and 9; Eq. 7 is referred to herein as: BSM (analytical equation).

$$\delta_{Total} = \delta_{Linear} + \delta_{Nonlinear} \tag{7}$$

where:

$$\delta_{Linear} = \frac{FL_t^3}{48EI_s} + \frac{F\left(L_t - L_s\right)^3}{48E}\left(\frac{1}{I_p} - \frac{1}{I_s}\right) \tag{8}$$

$$\delta_{Nonlinear} = \frac{L_t}{4\beta Dr}\ln\left(\frac{4\alpha r}{4\alpha r - FL_t}\right) \tag{9}$$

where:
$\delta_{Nonlinear}$ is given in millimeters.

8. Comparison of Experimental Results and BSMs

Fig. 8 depicts a comparison between the mid-span load-displacement curves obtained in the experiments and (i) BSM with experimental moment-rotation stiffness: "BSM (indirect M-θ curves)"; (ii) BSM with moment-rotation stiffness given by Eq. 4: "BSM (M-θ equation)"; and (iii) analytical equation for BSM, Eq. 7: "BSM (analytical equation)." Note that all methods lead to very similar and accurate prediction of displacement in the purlin-sleeve system.

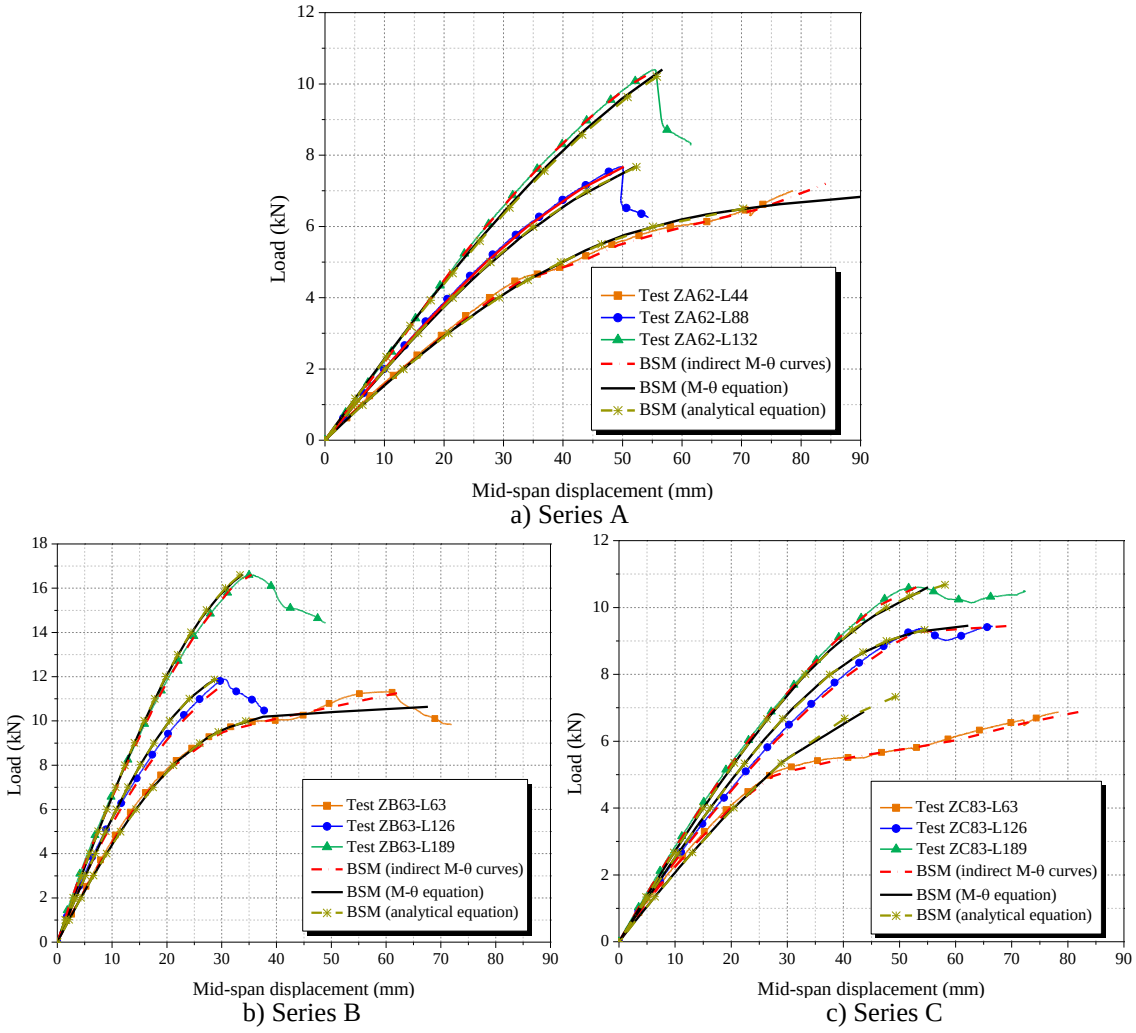

a) Series A

b) Series B

c) Series C

Figure 8: Comparison between BSM and experimental results.

9. The Use of Different Sleeve Thicknesses

Fig. 9 depicts curve force versus mid-span displacement for the experimental series with sleeve thickness of 1.95 mm (ZB63-L126 and ZC83-L126) and sleeve thickness of 3.00 mm (ZB63-L126T3 and ZC83-L126T3). In addition, the graph plots data for the respective continuous purlins experiment (ZB63-C and ZC83-C) and BSM that uses the moment-rotation stiffness determined experimentally. Note that sleeves of 3 mm lead to results very similar to the

continuous purlin experiment and that the BSM is able to accurately predict, in both cases, the purlin-sleeve system mid-span displacement.

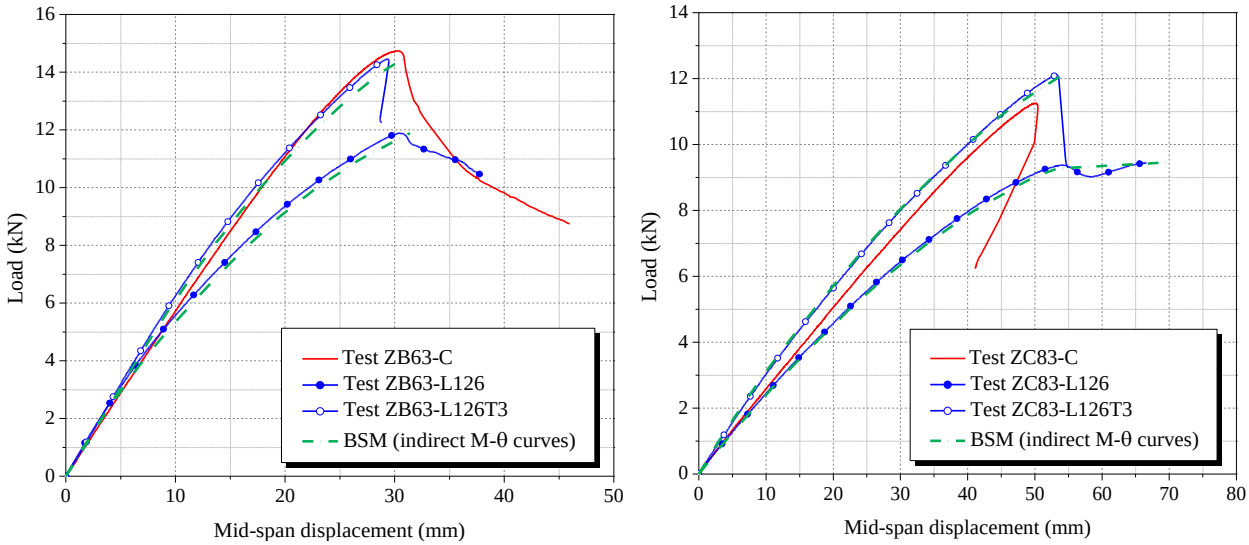

a) Series B b) Series C

Figure 9: Mid-span force-displacement curves for different sleeve thicknesses

Fig. 10 depicts the calibrated M-θ curves used in the BSM in Fig. 9. Note that the increase in purlin-sleeve system stiffness is led by the use of a different M-θ curve for each sleeve thickness.

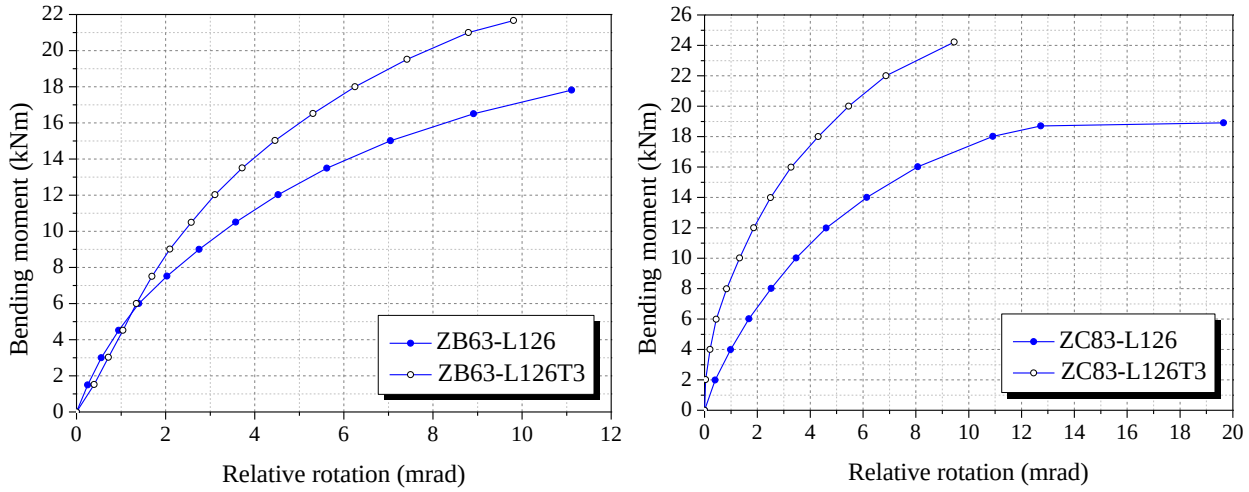

a) ZB63-L126 and ZB63-L126T3 b) ZC83-L126 and ZC83-L126T3

Figure 10: Moment-relative rotation curves

A similar conclusion can be drawn from experiments carried out by Fávero Neto et al. (2016) and additional experiments carried out by the authors of the present study using the same setting, but varying the thickness from 1.75 mm (ZD62-L1036) to 3.00 mm (ZE62-L1036), as in Fig. 11. BSM is also able to accurately predict system behavior in these cases.

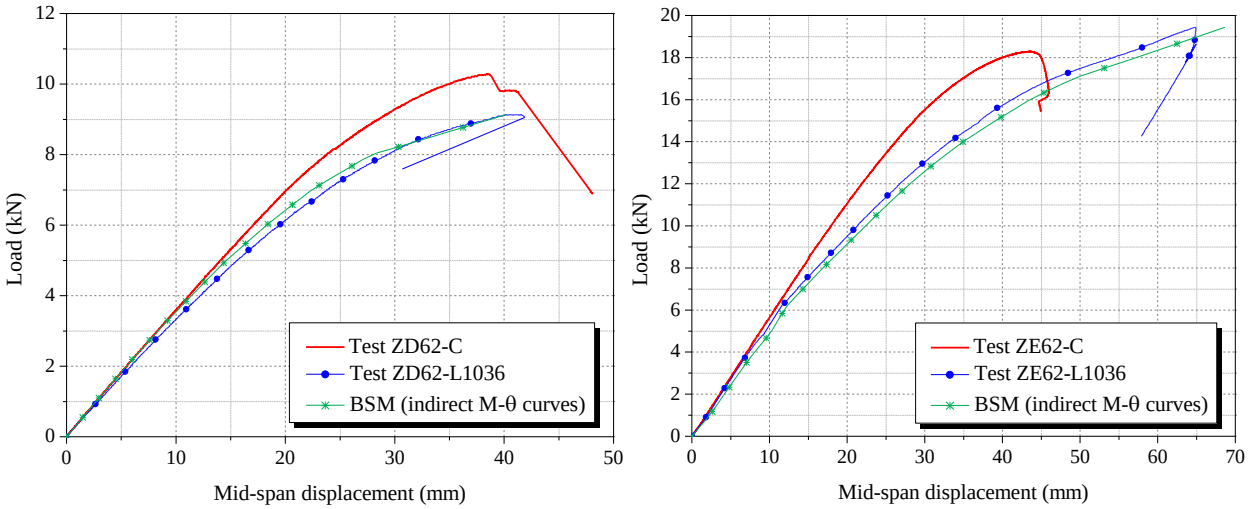

a) Series D b) Series E

Figure 11: Mid-span force-displacement curves

10. The Failure Mechanism

Continuous purlins failed in distortional buckling (ZA62-C) and local buckling (ZB63-C and ZC83-C) at the mid-span, as in Fig. 12a. The purlin-sleeve system failure mechanism switched from failure at the center of the sleeve (S1 section) to failure of the purlin near the connection end (S2 section), as shown, respectively, in Fig. 12b and 12c.

The demand in the sleeve-purlin systems with short size sleeve (Lp/D = 2) is similar at the center and at the end of the sleeve. The failure, however, mostly occurs at the purlin, since the sleeve is stiffened by the loading apparatus. For intermediate and long size purlin-sleeve systems (Lp/D = 4 and Lp/D = 6), the demand at the center of the system and at the end of the sleeve is considerably different. Thus, failure is predominantly at the center of the purlin-sleeve system, although the loading apparatus stiffens the sleeve, as in Fig. 12c.

The sleeve failed only at its own end in experiment ZC83-L63, Fig. 13, which led to a purlin-sleeve system stiffness lower than expected. This observation may be explained by an eventual problem during the assembly process.

Distortional buckling (Experiment: ZA62-C)

Local buckling (Experiments: ZB63-C e ZC83-C)

a) Continuous purlins

Local buckling of the purlin at the connection end
(Experiments: ZA62-L44, ZA62-L88, ZA62-L132, ZB63-L63, ZB63-L126T3 e ZC83-L126T3)

b) Short sleeve (Lp/D = 2) and purlin with sleeve thickness of 3.00 mm

Local bucking at the middle of the sleeve
(Experiments: ZB63-L126, ZB63-L189, ZC83-L126 e ZC83-L189)

c) Sleeve of intermediate size (Lp/D = 4) and long sleeve (Lp/D = 6)

Figure 12: Failure modes

Figure 13: Failure mechanism at the end of the sleeve ZC83-L63

11. Example Using Different Design Procedures

To clarify how structural engineers can use the models proposed herein, the authors present a practical design example. The example, shown in Fig. 14, is a beam with ten continuous and identical spans with 12 m length (L=12 m), in which a uniform load of 1.5 kN/m (q=1.5 kN/m) is applied, the Young's modulus is taken as equal to 200,000 MPa (E=200,000 MPa), and the cross-sectional dimensions are similar to the dimensions in the series B experiments (H=315 mm, t=1.89 mm, and I=13,433,260 mm^4).

An FE model of the system was analyzed using ANSYS; the model consists of beam elements (BEAM3), connected with non-linear rotational springs (COMBIN39), and linear rotational springs (COMBIN40). The spring elements aim to simulate the moment-rotation stiffness of the sleeve-purlin connection; at the region where purlin and sleeve overlap, the moment of inertia is considered equal to twice the purlin moment of inertia.

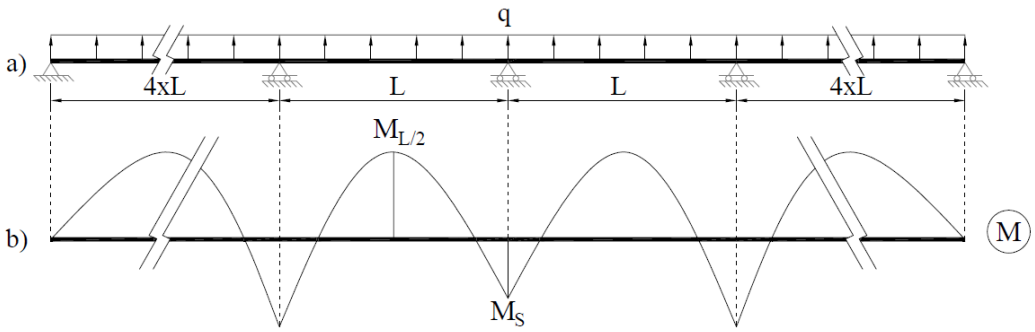

Figure 14: Example: a) multi-span system, and b) moment diagram of a continuous purlin

To study different design procedures, four models are investigated below:

i) Model 1 (reference) is composed of beam elements and a non-linear rotational spring with stiffness K_θ placed on the supports, as in Fig. 15. The spring stiffness values used in this model are the same as those depicted in Fig. 6.

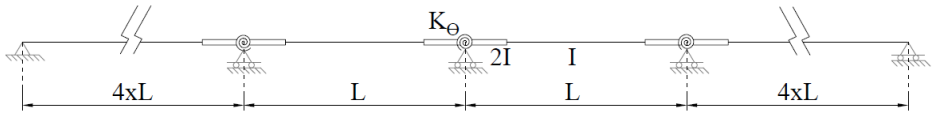

Figure 15: Model 1

ii) Model 2 is similar to Model 1, but the rotational stiffness K_θ is calculated using Eq. 3.

iii) Model 3 is composed of beam elements and two linear rotational springs positioned at the projection of each purlin to sleeve connection center, as in Fig. 16. Rotational stiffness K_θ is calculated via Eq. 1a; bearing stiffness at the bolt hole (K_h) is calculated according to Eq. 1b, Bryan (1993), and n is equal to 3.

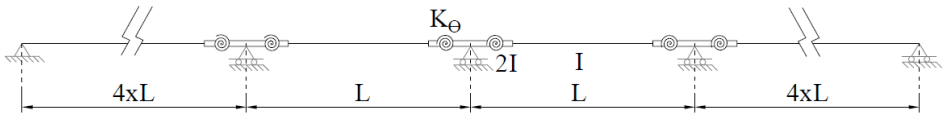

Figure 16: Model 3

iv) Model 4 is a linear-elastic model, which disregards the semi-rigid connection provided by the sleeve-purlin connection, as in Fig. 17.

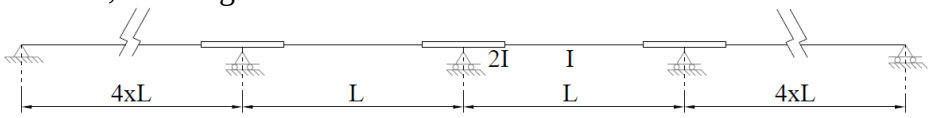

Figure 17: Model 4

Table 3 and Fig. 18 depict the analysis results for different sleeve sizes, but the same cross-section, material, and span as mentioned above. Bending moment at the center support (M_S) and maximum bending moment in between supports ($M_{L/2}$) are reported in Table 3. Note that: (i) the greater the sleeve length, the greater is the moment at the center support and the lower it is in between supports; (ii) in Model 4 (no rotational springs) bending moment is greatest at the center support, followed by Model 2 (rotational spring stiffness is calculated using Eq. 3), Model 1 (empirical rotational spring stiffness), and Model 3 (rotational spring stiffness calculated using Eq. 1.b, Bryan (1993)); and (iii) there is a clear balance between M_S and $M_{L/2}$, which is useful for structural design engineers who aim to maximize cross-section efficiency by having the M_S value close to the $M_{L/2}$ value.

Table 3: Bending moment at different positions

	Experiment	**ZB63-L63**		**ZB63-L126**		**ZB63-L189**	
	Moment (kN.cm)	**M_S**	**$M_{L/2}$**	**M_S**	**$M_{L/2}$**	**M_S**	**$M_{L/2}$**
Model	1	1494	1206	1670	1031	1805	900
	2	1514	1186	1703	998	1815	891
	3	1284	1416	1676	1028	1827	881
	4	1856	854	1897	815	1933	781

Fig. 18 depicts purlin-sleeve system stiffness using different models studied in this example. For short sleeves, Fig. 18a, there is a clear difference between the models, except for Models 2, which are, independent of sleeve size (Fig. 18a, 18b and 18c), very similar with Model 1 (reference). For intermediate and long-size sleeves, Models 2 and 3 are similar, and one may conclude that Model 4 does not correctly represent the purlin-sleeve system behavior in any instance. On the other hand, Model 3, based on Bryan (1993), is acceptable only for systems that use intermediate and long sleeves.

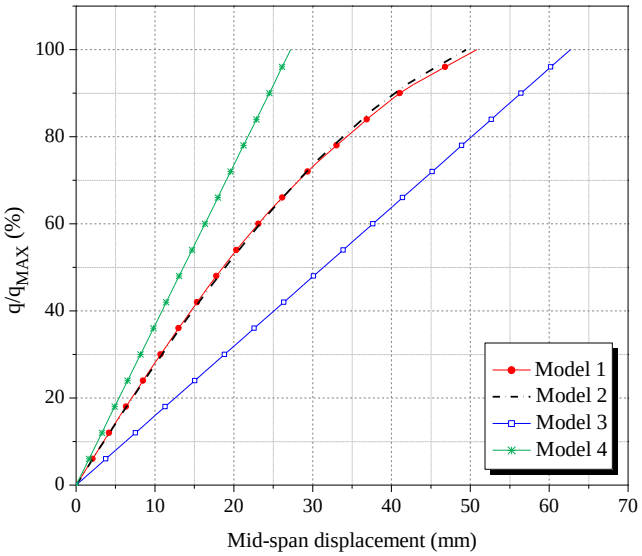

a) ZB63-L63 (L_p/D = 2)

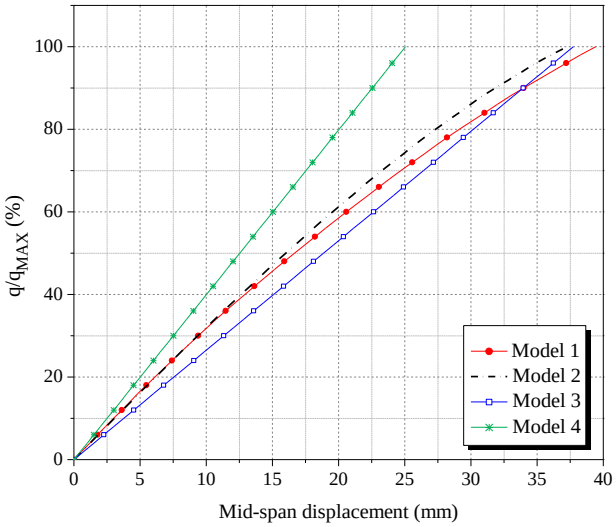

b) ZB63-L126 (L_p/D = 4)

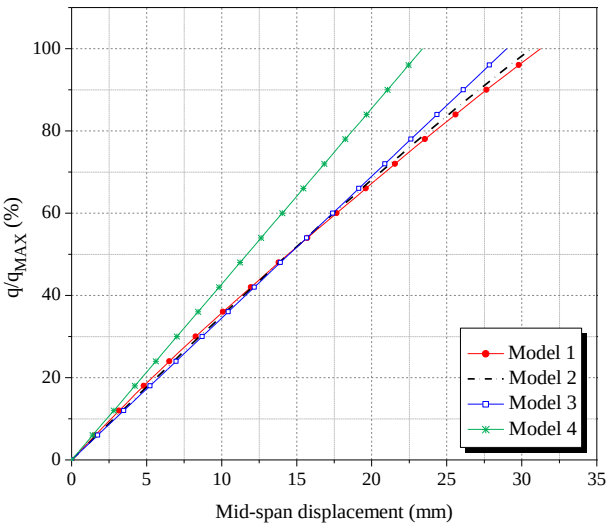

c) ZB63-L189 (L_p/D = 6)

Figure 18: Loading-displacement curves for the sleeve-purlin system (series B) (limit loading is set to peak load at the experimental analysis)

12. Conclusions

Fifteen experiments on cold-formed steel Z-section purlins with sleeved bolted connections tested in bending while varying cross-section height, thickness and length of sleeve, and span were carried out to better understand the flexural-buckling strength, collapse mechanism, and moment-rotation behavior of purlin-sleeve systems. Given the loading-displacement curves of the parametric experimental study and the literature review, it is clear the importance of taking into account the purlin-sleeve stiffness and strength of the system. A simplified superposition approach allowed the authors to divide the system stiffness into bending deformation stiffness and rigid-body translation, which led to calibrated simplified equations to predict the non-linear

relationship between moment and relative rotation, depicted by the moment-rotation (M-θ) curve. The simplified equation proposed herein is able to take into account: sleeve effective length, cross-section height, and span. The proposed equation used in conjunction with FE models (classic beam element and non-linear spring element) lead to accurate prediction of system displacement at any loading stage. This parametric experimental study also shows that failure mechanisms are sensitive to sleeve length; for short sleeve lengths, the loading apparatus length may interfere with the failure position and ultimate load, which is not an issue for intermediate and long sleeves. Note that the loading apparatus is designed to be similar to a typical structural frame in which the sleeve is attached. Further research should be carried out to accurately predict the purlin-sleeve system ultimate load.

Acknowledgements

The authors are indebted to Coordination for the Improvement of Higher Education Personnel (CAPES) and National Council for Scientific and Technological Development (CNPq) for funding and Modular Building Systems for donating the specimens.

References

ABNT, NBR 14762 (2010): "Design of cold formed steel structures.", Rio de Janeiro.

ASTM, A325 (2013). "Standard specification for structural bolts, steel, heat treated 830 MPa minimum tensile strength (Metric)." West Conshohocken, PA.

ASTM, A370 (2014). "Test methods for tension testing of metallic materials." West Conshohocken, PA.

Bryan, E. R. (1993). "The design of bolted joints in cold-formed steel sections." *Thin-Walled Structures*, v. 16, p. 239-262.

Fávero Neto, A. H.; Vieira JR., L.C.M.; Malite, M. (2016). "Strength and stiffness of cold-formed steel purlins with sleeved and overlapped bolted connections." *Thin-Walled Structures*, v. 104, p. 44-53.

Ghosn, A. A.; Sinno, R.R. (1996). "Load capacity of nested, laterally braced, cold-formed steel Z-section beams." *Journal of Structural Engineering*, v. 122, p. 968-971.

Gutierrez, R.; Loureiro, A.; Lopez, M.; Moreno, A. (2011). "Analysis of cold-formed purlins with slotted sleeve connections." *Thin-Walled Structures*, v.49, p. 833-841.

Gutierrez, R.; Loureiro, A.; Reinosa, J. M.; Lopez, M. (2015). "Numerical study of purlin joints with sleeve connections." *Thin-Walled Structures*, v. 94, p. 214-224.

Moore, D. B. (1990). "Moment-rotation characteristics of purlin connections." In: *Proceedings of 10th International Specialty Conference on Cold-formed Steel Structures*. Saint Louis. University of Missouri Rolla. p. 525-544.

Yang, J.; Liu, Q. (2012). "Sleeve connections of cold-formed steel sigma purlins." *Engineering Structures*, v. 43, p. 245-258.

Ye, W.; Wang, C. J.; Mynors, D. J.; Kibble, K. A.; Morgan, T.; Cartwright, B. (2013). "Load–deflection behavior of sleeved joints in modified Z purlin system." *Thin-Walled Structures*, v. 73, p. 318-328.